Catalysis Science & Technology

Accepted Manuscript

ROYAL SOCIETY OF CHEMISTRY

www.rsc.org/catalysis

Cite this: DOI: 10.1039/c0xx00000x

www.rsc.org/xxxxxx

ARTICLE TYPE

Cycloaddition of CO_2 and epoxide catalyzed by amino- and hydroxyl-rich graphitic carbon nitride

Zhijun Huang, Fengbo Li,* Bingfeng Chen and Guoqing Yuan*

Received (in XXX, XXX) Xth XXXXXXXXX 20XX, Accepted Xth XXXXXXXXX 20XX

DOI: 10.1039/b000000x

Graphitic carbon nitride (g-C_3N_4) shows great application potential in the activation of CO_2 due to its basic surface functionalities and highly specific electronic properties. Herein, to improve the catalytic performance, g-C_3N_4 was activated by protonation using H_2SO_4. The texture, surface chemistry and electronic properties of the as-prepared g-C_3N_4 were then studied. The synthesis of cyclic carbonate from the cycloaddition of CO_2 and epoxide was selected as a model reaction to investigate the catalytic performance. The protonated g-C_3N_4 exhibited much higher catalytic activity than that of the pristine g-C_3N_4. The generation of terminal amino and hydroxyl groups due to the hydrolysis of g-C_3N_4 under acidic condition as well as the higher specific surface area is responsible for the enhanced catalytic performance.

Currently, 80 to 85% of the world's commercial energy depends on carbon-based fossil fuels.[1] The consumption of fossil fuels produces large amounts of CO_2, which was proved to be the main reason for the greenhouse. Indeed, the CO_2 concentration in atmosphere has increased from 278 ppm during the preindustrial era to above 400 ppm in 2015. In view of the fact that CO_2 is an inexpensive, nontoxic and abundant carbon source, the use of CO_2 as a starting carbon feedstock for useful chemicals is a practical route to reduce its accumulation.[2] However, CO_2 is both thermodynamically and kinetically stable, and is not used in large-scale in modern industry. The difficulty of CO_2 activation is the key-limiting factor for its utilization. Therefore, catalyst, often a metal system, is required to tackle this issue.

Recently, graphitic carbon nitride (g-C_3N_4), a metal-free organic semiconductor has attracted widespread attention due to its potential applications in heterogeneous (photo)catalysis.[3,4] This highly stable and abundant polymer is composed of tri-*s*-triazine units connected through trigonal nitrogen atoms. The unique chemical composition provides g-C_3N_4 with a large amount of basic functional groups, including both Lewis base and Brönsted base.[5] These basic functions may act as nucleophilic sites for the activation of CO_2. By careful design of the catalytic active sites, a photocatalyst system consisting of a Ru complex and g-C_3N_4 was developed for the reduction of CO_2 into formic acid. A turnover numbers (TON) above 1000 with respect to Ru was achieved under visible light irradiation for 20 h.[6] Except for formic acid, other useful chemicals, such as CO,[7] methane, [8] methanol [9] and acetaldehyde [10] were also synthesized using different g-C_3N_4 based photocatalysts. Even without the light irradiation, CO_2 can be activated by g-C_3N_4 to form $O^{\cdot\cdot}$ diradical, which subsequently react with benzene to form phenol.[11] However, compared with metal catalysts, the catalytic efficiency of g-C_3N_4 for the activation of CO_2 is still very low and not suitable for practical applications.[12] The synthesis of cyclic carbonate from the cycloaddition of CO_2 and epoxide is an exception. It was reported that, g-C_3N_4 can serve as an efficient catalyst for the fixation of CO_2 with epoxides.[13] The resulting cyclic carbonates have been widely used as aprotic solvents, electrolytes in lithium-ion batteries, monomer for polycarbonates and fuel additives.[14, 15] A moderate to excellent catalytic activity can be achieved by modulating the texture structure and surface chemical properties of g-C_3N_4. Heating urea at 480 to 550 ^oC, a series of g-C_3N_4 with different crystallinities was synthesized.[16] The as-prepared g-C_3N_4 obtained at lower temperature exhibited higher activity, which indicates that the amino groups derived from the incomplete condensation served as the main active sites in the activation of CO_2. The catalytic activity also can be improved significantly by modification of g-C_3N_4 with n-bromobutane [17] or metal halides [18]. The synthergistic effect of the uncondensed amino groups and halide anions were speculated to be the main reason.

In our previous studies, SBA-15 supported g-C_3N_4 nanophases were prepared by vapor condensation of dicyandiamide.[19] These nanostructures with strong Lewis basicity and optimized electronic properties exhibited exceptionally high catalytic activity for the synthesis of cyclic carbonates from CO_2 and epoxides. Multiple-step procedures involving the preparation of SBA-15, loading of dicyandiamide and subsequent condensation at high temperature are required to obtain this powerful catalyst. Therefore, a simple method for the synthesis of g-C_3N_4 catalyst with high activity is of particular interest. Recently, Zhang *et al*. developed a convenient route for the activation of g-C_3N_4 by protonation using HCl.[20] Protonation not only provides higher specific surface area and better dispersion, but also improves the electronic and surface chemical properties, which all benefit its catalytic applications.[21] Herein, to strengthen this positive effect, H_2SO_4, a stronger Brönsted acid was used to the activation of g-C_3N_4. The texture structures, surface chemistry and electronic properties of the resultant g-C_3N_4 were investigated. The catalytic

activity for the activation of CO_2 was also investigated by the cycloaddition of CO_2 with epichlorohydrin as a model reaction.

2. Experimental

2.1 Synthesis of catalysts

g-C_3N_4 was synthesized by heating melamine under still air. Typically, melamine was put into a covered crucible. The crucible was then heated to 550 ^oC in a muffle furnace for 4 h with a heating rate of 5 ^oC min^{-1}. After the reaction, the crucible was cooled down to room temperature. The obtained g-C_3N_4 was ground to a powder.

g-C_3N_4-S was synthesized by protonation of pristine g-C_3N_4 with H_2SO_4. Typically, 1 g of g-C_3N_4 was stirred with 15 ml of H_2SO_4 (60%) at 80 ^oC for 2 h. The obtained yellow suspension was added drop by drop to 50 ml of deionized water under an ice-water bath. The protonated g-C_3N_4 was collected through centrifugation, washed thoroughly with water and ethanol and drying at 60 ^oC in vacuum overnight. For comparison, g-C_3N_4 was also treated with H_2SO_4 at 40 and 60 ℃, and the products were denoted as g-C_3N_4-S-40 and g-C_3N_4-S-60 respectively.

2.2 Characterization

Transmission electron microscopy (TEM) images were recorded on a JEOL JSM-2100 instrument with an accelerating voltage of 200 kV. Nitrogen adsorption–desorption experiments were carried out at 77.3 K by a Quanta-chrome Autosorb Automated Gas Sorption System (Quantachrome Corporation). Powder X-ray diffraction (XRD) were performed on a Rigaku Rotaex diffractometer equipped with Cu Kα radiation source (40 kV, 200 mA; λ=1.54056 Å). Fourier transform infrared (FT-IR) spectra were collected on a Bruker Tensor 27 by using KBr pellets. X-ray photoelectron spectroscopy (XPS) dates were recorded on a Thermo Scientic ESCALab 250Xi using 200 W monochromated Al Kα radiation. UV-visible absorption spectra were obtained on a Shimadzu UV-2600 UV-visible spectrometer equipped with an integrating sphere assembly. Photoluminescence (PL) spectra were recorded on a Hitachi F-4500 fluorescence spectrometer. Electron paramagnetic resonance (EPR) experiments were carried out on a Bruker E500 spectrometer. Elemental analysis experiments were performed on a Flash EA 1112.

2.3 Cycloaddition of CO_2 with epoxide

The cycloaddition reactions were carried out in a 100 ml stainless steel autoclave equipped with a magnetic stir bar. The catalysts (50 mg) and epichlorohydrin (5 ml) were successively introduced into the reactor. The reactor was purged with N_2 three times and then heated to 90 - 140 ^oC, and maintained for 20 min. Thereafter, the reactor was pressurized with CO_2 to 0.5 - 4.5 MPa and stirred for 2 h before cooled to 0 ^oC in ice water. The catalysts were separated by centrifugation and the products were analyzed by a gas chromatograph (GC-2014, SHIMADZU) equipped with an FID detector.

3. Results and discussion

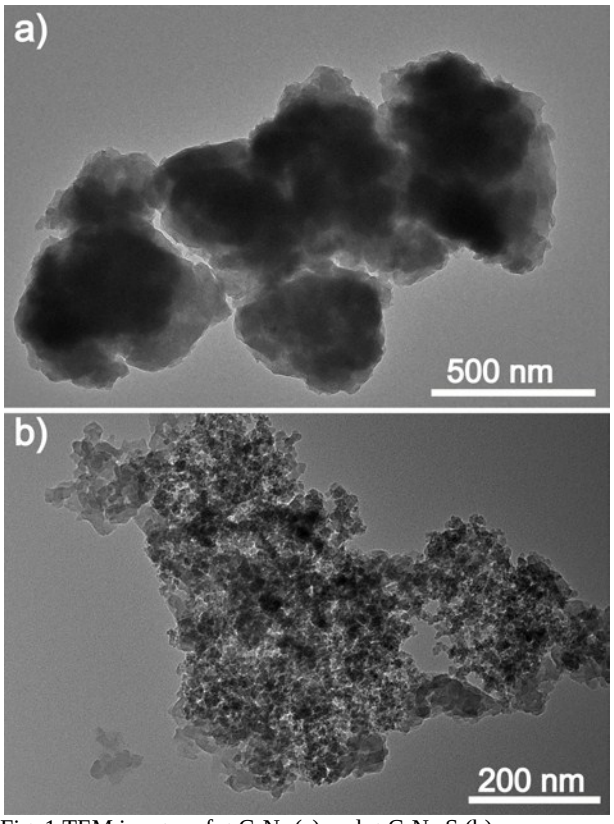

Fig. 1 TEM images of g-C_3N_4 (a) and g-C_3N_4-S (b).

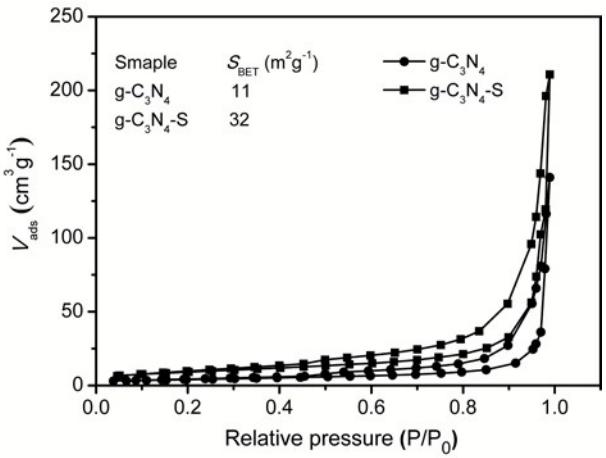

Fig. 2 N_2 adsorption–desorption isotherms of g-C_3N_4 and g-C_3N_4-S.

3.1 Effect of protonation on structure, composition and electronic properties

The morphologies of g-C_3N_4 before and after protonation were investigated by TEM. As shown in Fig. 1a, the g-C_3N_4 obtained by direct heating melamine is solid agglomerate with several hundred nanometers in size. This pristine g-C_3N_4 was disintegrated into smaller particles after protonation with H_2SO_4, and its size reduced to 20 to 50 nm as exhibited in Fig. 1b. The morphological change results in a large amount of structural defects. These defects may provide more catalytic active sites for the adsorption and activation of CO_2.

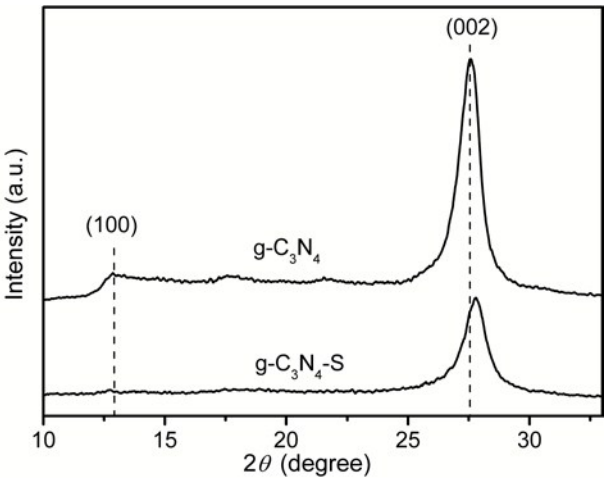

Fig. 3 Powder XRD patterns of g-C_3N_4 and g-C_3N_4-S.

Nitrogen adsorption–desorption experiments were preformed to analyze the porous information. Fig. 2 shows the isotherm curves of the samples before and after protonation. Similar to the pristine g-C_3N_4, g-C_3N_4-S displays a typical type III isotherm. The H3 hysteresis loop located at $0.35 < P/P_0 < 1.00$ indicates the existence of open pores, which are stemmed from the agglomeration of particles. [22] The BET specific surface area (S_{BET}) of g-C_3N_4-S was calculated to be 32 m^2g^{-1}, much higher than that of the pristine g-C_3N_4 (11 m^2g^{-1}).

The crystal structures were measured by XRD. As can be seen from Fig. 3, the pristine g-C_3N_4 prepared from melamine shows two characteristic diffraction peaks at 2θ = 27.5° and 13.1°. The former is ascribed to the interlayer stacking structure (002), and the later belongs to the in-planar repeating tri-*s*-triazine units (100). g-C_3N_4-S was found to have the same (002) diffraction peak as the pristine g-C_3N_4, suggesting that the interlayer stacking structure has not been destroyed during treatment with H_2SO_4.[23] However, the formation of structural defects after protonation leads to a decreased crystallinity. As a result, the intensity of the (002) peak tends to be weaker.[24] For the same reason, the (100) peak also becomes less pronounced for g-C_3N_4-S.

The generation of structural defects during protonation was also revealed by FT-IR spectra presented in Figure 4. The absorption band in 3000–3600 cm^{-1} is obviously enhanced for g-C_3N_4-S, which indicates that some terminal amino groups (–NH_2 or =NH groups) were generated during protonation.[25] Due to the excellent chemical inertness of the tri-*s*-triazine units, the core chemical structure of g-C_3N_4 is rather stable against acid etching. No evident change in the absorption band at 809 cm^{-1} and 1200–1650 cm^{-1} ascribed to the tri-s-triazine units and the aromatic CN heterocycles respectively was found.[26] XPS measurements further confirmed the formation of terminal amino groups. As shown in Fig. 5, the XPS spectra of N1s were fitted into three peaks at 398.4 eV, 399.8 eV and 400.9 eV, corresponding to sp^2-hybridized nitrogen in tri-*s*-triazine rings (C–N=C), tertiary nitrogen N–$(C)_3$ groups and amino groups (–NH_2 or =NH), respectively.[27] The content of nitrogen in the amino groups for g-C_3N_4 is 7.3%. Due to the generation of terminal amino groups during protonation as demonstrated by FT-IR results, this value is increased largely to 14.2% for g-C_3N_4-S.

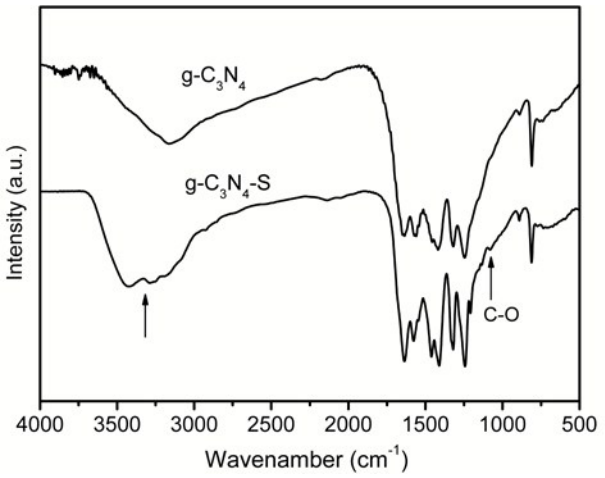

Fig. 4 FT-IR patterns of g-C_3N_4 and g-C_3N_4-S.

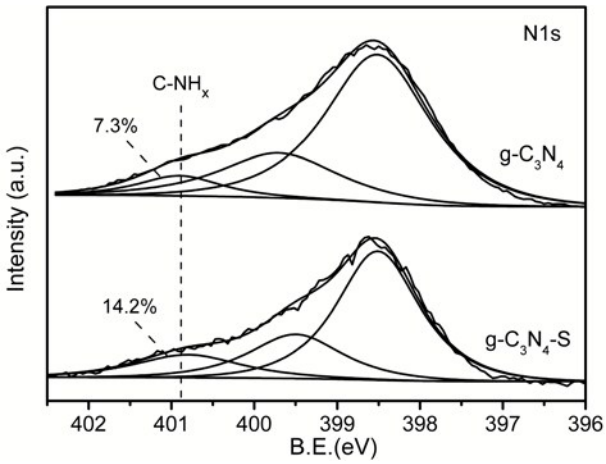

Fig. 5 N1s XPS peaks of g-C_3N_4 and g-C_3N_4-S.

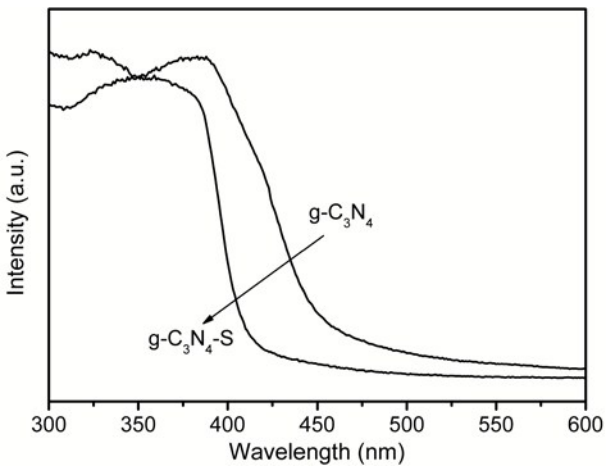

Fig. 6 UV-visible absorption spectra of g-C_3N_4 and g-C_3N_4-S.

The protonation process remarkably modified the electronic structure of g-C_3N_4. As shown in Fig. 6, the absorption edge of the pristine g-C_3N_4 is about 440 nm. After protonation with H_2SO_4, the absorption edge of g-C_3N_4-S is blue-shifted to about 400 nm. The change in the light absorption can be presumably ascribed to the strong quantum confinement effect due to the reduced size.[28] In addition, the decrease in the crystallinity owing to the formation of structure defects is another reason for this

change.[24] The PL spectra show a similar result as that of the UV-visible absorption spectra.[29] As presented in Fig. 7, the emission peak of pristine g-C_3N_4 is about 460 nm. After protonation, the emission peak is blue-shifted to about 423 nm. Furthermore, a slightly decreased PL intensity of g-C_3N_4-S was observed. This indicates that the efficiency in the migration, transfer and separation of the photogenerated charge carriers was enhanced.

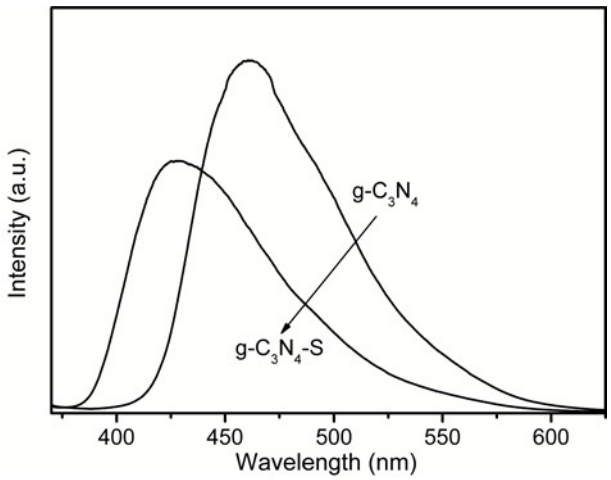

Fig. 7 PL spectra of g-C_3N_4 and g-C_3N_4-S.

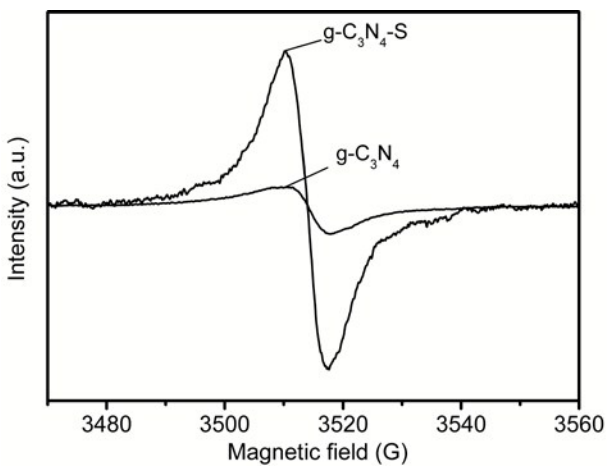

Fig. 8 EPR spectra of g-C_3N_4 and g-C_3N_4-S.

The electronic structure information was further studied by solid-state EPR at room temperature. As shown in Fig. 8, both g-C_3N_4 and g-C_3N_4-S exhibit one single Lorentzian line with a *g* value of 2.0033. It is clear that, the EPR signal of g-C_3N_4-S is much stronger than that of g-C_3N_4. According to the literatures, [30,31] the EPR signal is originated from the unpaired electrons in the aromatic rings of carbon atoms, which is located at the nanoclusters on the surface of the materials. Obviously, the large S_{BET} and the structure defects of g-C_3N_4-S are responsible for the enhanced EPR signal. [32]

3.2 Synthesis of cyclic carbonate from the cycloaddition of CO_2 and epoxide

The synthesis of cyclic carbonate from the cycloaddition of CO_2 and epoxide was employed for evaluating the catalytic performance of the protonated g-C_3N_4 (Table 1). Epichlorohydrin was chosen as a model substrate in the reaction. In the absence of catalyst, the reaction hardly occurs. After the introduction of g-C_3N_4, a conversion of 5.6% was achieved after 2 h, suggesting g-C_3N_4 can catalyze the cycloaddition reaction. The selectivity of chloropropyl carbonate was 96.7%. Diol was found to be the main by-products. It is clear that the protonated g-C_3N_4 showed much higher activity than that of the pristine g-C_3N_4. For g-C_3N_4-S, the conversion of epichlorohydrin was 99.1%, more than 17 times higher than that of pristine g-C_3N_4. As the conversion increased, the hydrolysis of epoxide to diol was suppressed.[33] As a result, the selectivity of chloropropyl carbonate was increased to 99.5%. When the reaction time was prolonged to 3 h, almost all the epichlorohydrin was consumed. The yield of chloropropyl carbonate reached 99.4%. To be completely convincing of the positive effect of protonation, the cycloaddition reaction was also catalyzed by g-C_3N_4 treated with H_2SO_4 at 40 and 60 °C respectively. The results show that the catalytic activity increased successively with the increase in treating temperature between 40 and 80 °C. However, by further increasing the temperature to 100 °C, g-C_3N_4 could be dissolved in H_2SO_4 to form a clear solution. [23, 25]

Table 1 Catalytic performance of different catalysts.[a]

Catalyst	Conv. (%)	Sel. (%)	Yield (%)
—	<1	—	<1
g-C_3N_4	5.6	96.7	5.4
g-C_3N_4-U	6.1	97.9	8.1
g-C_3N_4-S	99.1	99.5	98.6
g-C_3N_4-S [b]	>99.9	99.4	99.4
g-C_3N_4-S-40	26.9	98.8	26.6
g-C_3N_4-S-60	57.2	99.6	57.0

[a] Reaction conditions: epichlorohydrin (5 ml), catalyst (50 mg), temperature (130 °C), CO_2 pressure (3.5 MPa), time (2 h). [b] Time (3h).

Table 2 Comparison of typical g-C_3N_4 catalysts reported for cycloaddition of CO_2 and epoxides.

Catalysts	Epoxides	*T* (°C)	*P* (MPa)	Conv. (%)	TOF (h^{-1})
g-C_3N_4	ECH [a]	130	3.5	5.6	3.3
g-C_3N_4-S	ECH[a]	130	3.5	99.1	58.1
MS-MCN[13]	PO[b]	100	0.55	34.0	3.4
u-g-C3N4-480[16]	ECH[a]	130	2.0	99.6	4.9
n-butBr/mp-C_3N_4[17]	PO[b]	140	2.5	88.0	9.6
$ZnCl_2$/mp-C_3N_4[18]	PO[b]	140	2.5	73.0	5.6
g-C_3N_4/SBA-15[19]	SO[c]	150	3.5	94.5	15.2

[a] ECH: Epichlorohydrin, [b] PO: Propylene oxide, [c] SO: Styrene oxide.

The turnover frequencies (TOF) of pristine g-C_3N_4 and g-C_3N_4-S are calculated and summarized in Table 2. The TOF of pristine g-C_3N_4 is 3.3 h^{-1}. This value is increased to 58.1 h^{-1} for g-C_3N_4-S. For comparison, the catalytic performances of several g-C_3N_4 catalysts reported for cycloaddition of CO_2 and epoxides are listed. The highest activity is provided by g-C_3N_4/SBA15, which exhibits a TOF value of 15.2 h^{-1}. g-C_3N_4-S is more than 3 times more efficient than g-C_3N_4/SBA15 in terms of TOF, suggesting that the present protonated g-C_3N_4 is really a highly efficient

catalyst.

The effects of reaction temperature and pressure on the cycloaddition reaction were investigated. As shown in Fig. 9a, the temperature had a positive effect on the reaction. Only a low conversion of 15.4% was obtained at 90 °C. The conversion increased sharply to 99.1% with an increase in the temperature to 130 °C. It remained at this level when the temperature was elevated to 140 °C. Further increase in the temperature may result in the polymerization of chloropropyl carbonate, which reduced the selectivity of the target product.[34, 35] The fluctuating of the CO_2 pressure does not affect the reaction rate as markedly as the temperature. As shown in Fig. 9b, the cycloaddition reaction can proceed smoothly even under 0.5 MPa. The conversion of epichlorohydrin increased gradually from 48.7% to 99.3% with the increase of pressure from 0.5 to 4.5 MPa. The higher conversion at elevated pressure may be associated with the increased CO_2 concentration within the reaction system.[36]

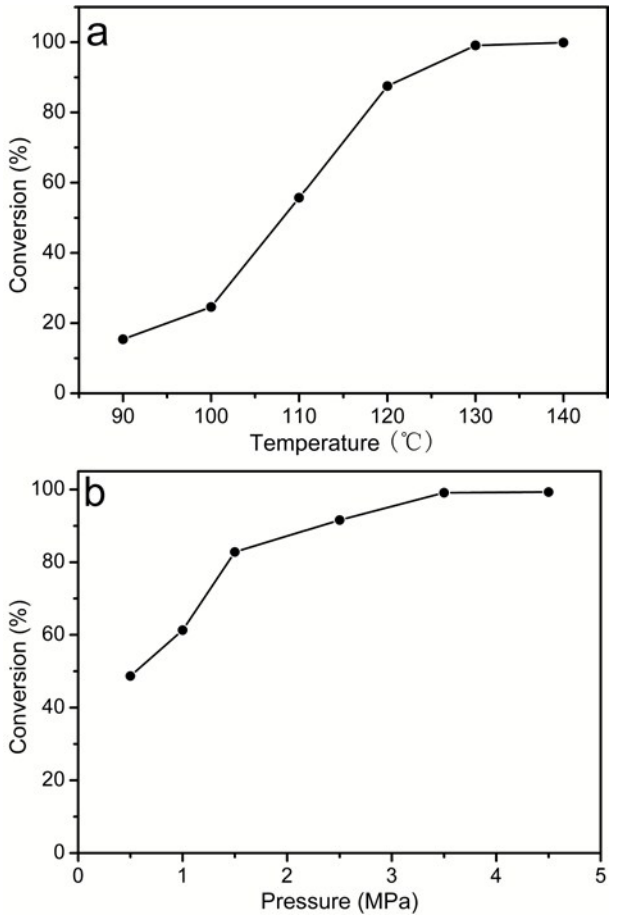

Fig. 9 Effects of reaction temperature (a) and CO_2 pressure (b) on the catalytic performances of g-C_3N_4-S. Reaction conditions: epichlorohydrin (5 ml), catalyst (50 mg), time (2 h); CO_2 pressure (3.5 MPa) for (a) and temperature (130 ℃) for (b).

3.3. The correlation between catalytic performances and surface functional groups

The improved catalytic performance of the protonated g-C_3N_4 is partly due to its high S_{BET}. The high S_{BET} could not only provide more catalytic active sites, but is also beneficial for the adsorption and diffusion of reactants, thus accelerating the reaction.[37] However, when g-C_3N_4-U, a g-C_3N_4 material with a high S_{BET} of 64 m^2g^{-1} was used as a catalyst, only a low conversion of 8.1% was obtained. This strongly demonstrates that S_{BET} is not the sole or even the predominant reason for the enhanced catalytic activity. It was pointed out that, terminal amino groups derived from the structure defect of g-C_3N_4 are the active sites in catalytic reactions.[11,16,38] According to the results and discussions depicted above, terminal amino groups would be generated during protonation. Therefore, we speculate that the generation of terminal amino groups is another reason for the enhanced catalytic performance.

Table 3 Stoichiometries of g-C_3N_4 and g-C_3N_4-S deterimined by elemental analysis

Smaples	C	N	H	O	C/H [a]	C/O [a]
g-C_3N_4	3	4.47	1.86	0.15	1.61	20.00
g-C_3N_4-S	3	4.47	4.38	0.36	0.68	8.33

[a] atomic ratio

However, compared with the enhanced catalytic activity (17.7 times), the value of the increased S_{BET} (2.9 times) and terminal amino group (1.9 times) are relatively low. This implies that some other factors may be also responsible for the high catalytic activity. It was reported that protonation may lead to the hydrolysis of g-C_3N_4.[39] As a result, some surface functional groups, such as amino and hydroxyl groups were generated.[40] The generation of amino groups was already demonstrated by FT-IR and N1s XPS measurements. The generation of hydroxyl groups can be illuminated by elemental analysis. As shown in Table 3, The C/H atomic ratio was decreased from 1.61 for g-C_3N_4 to 0.68 for g-C_3N_4-S. The C/O atomic ratio was decreased from 20.00 for g-C_3N_4 to 8.33 for g-C_3N_4-S. The treatment with H_2SO_4 increased the content of H and O significantly due to the generation of hydroxyl groups through partial hydrolysis of g-C_3N_4. The increase in the O content was also confirmed by XPS survey spectrum. As shown in Fig. 10a, the pristine g-C_3N_4 is mainly composed of C and N elements. A small amount of O (5.1%) also appeared. After protonation with H_2SO_4, the content of O was increased to 9.4%. The adsorption of water may also lead to an increase in the content of H and O. To exclude the effect of the adsorbed water, the chemical state of O was further identified by O1s XPS spectra. As exhibited in Fig. 10b, the O1s spectrum of g-C_3N_4-S was fitted into two peaks. The peak at 533.2 eV is ascribed to the adsorbed H_2O, and the peak at 531.8 eV is ascribed to the hydroxyl group.[41,42] In contrast, only one peak at 533.2 eV, which is ascribed to the adsorbed H_2O, is appeared in g-C_3N_4. The same result was further confirmed by FT-IR spectra. As shown in Fig. 4, a new signal located at 1086 cm^{-1}, which is ascribed to the C-O, appeared after protonation.[43] Thus, it can be ascertained that some hydroxyl groups was generated during hydrolysis of g-C_3N_4 under acidic condition.

It is generally accepted that g-C_3N_4 is very active for the activation of CO_2 through acid-base coupling. But for the activation of epoxide, the activity is relatively low. To catalyze the cycloaddition of CO_2 and epoxides by g-C_3N_4, co-catalysts were usually employed to activate epoxides.[17,18] It has been known that the formation of hydrogen bond between hydroxyl

groups and the oxygen atom of epoxides is a key step for the activation of epoxides by graphite oxide [44,45], cellulose,[46,47] and hydroxyl-functionalized ionic liquids [48]. Thus, we proposed that the hydroxyl group derived from the hydrolysis of g-C_3N_4 is the third reason for the high catalytic activity.

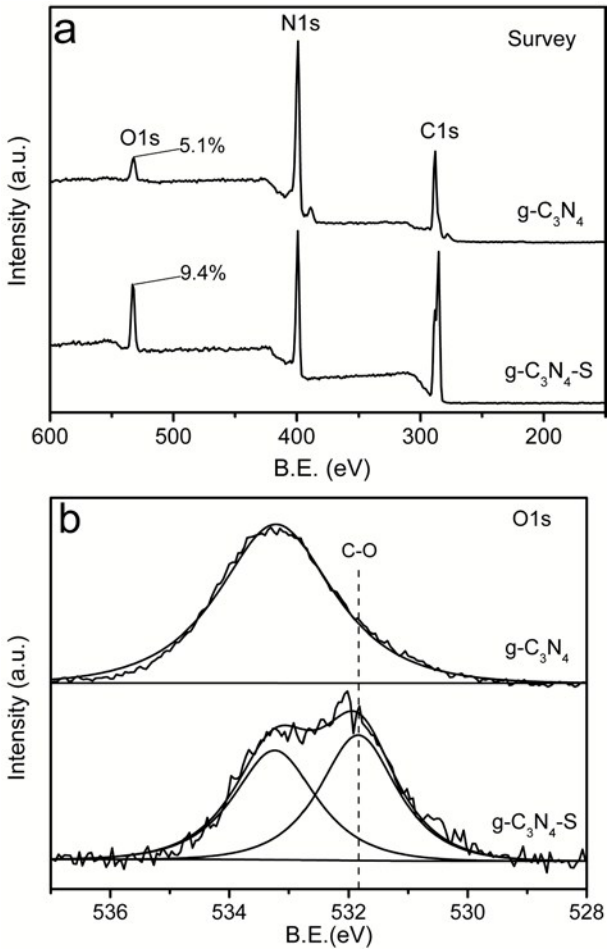

Fig. 10 XPS survey spectra (a) and O1s spectra (b) of g-C_3N_4 and g-C_3N_4-S.

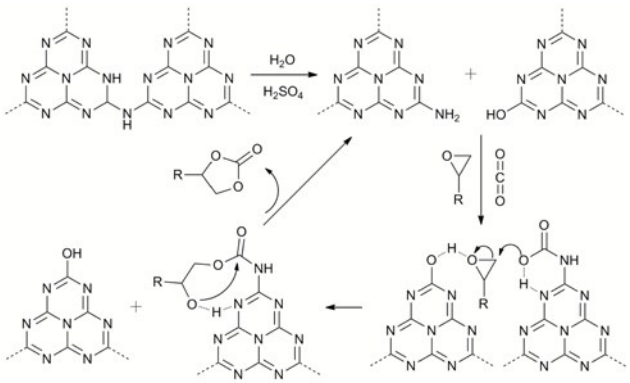

Scheme. 1 Generation of active sites and possible mechanism for the cycloaddition of CO_2 with epoxide.

The generation of active sites and the subsequent activation of reactants and formation of cyclic carbonate are illustrated in scheme 1. Firstly, g-C_3N_4 was partially hydrolyzed during treatment with H_2SO_4. Amino and hydroxyl groups were generated. After the reactants were added, the epoxide was activated by hydroxyl group through hydrogen bond. At the same time, CO_2 was activated by amino group, and a carbamate species was formed. Subsequently, the activated CO_2 attacked on the less hindered carbon atom of the activated epoxide. Therefore, ring opening occurred. Finally, cyclic carbonate was produced through subsequent intramolecular ring-closure, and the catalyst was regenerated simultaneously.

In conclusion, g-C_3N_4 was successfully activated by protonation using H_2SO_4. The texture, surface chemistry and electronic structure were optimized during protonation. The protonated g-C_3N_4 is a very active catalyst for the synthesis of cyclic carbonate from the cycloaddition reactions of CO_2 with epoxide. The catalytic activity of g-C_3N_4 protonated by H_2SO_4 at 80 ^oC is 17.7 times higher than that of pristine g-C_3N_4. The high specific surface area, the generation of terminal amino groups and especially hydroxyl groups maximize the catalytic potential of g-C_3N_4. It is highly expected that the facile synthesis method and the excellent catalytic performance makes protonated g-C_3N_4 a good candidate for further applications in the utilization of CO_2 as a carbon feedstock for the production of useful chemicals.

Acknowledgements

This work was supported by the National Natural Science Foundation of China (21304101, 21174148, 21403248, 21373234).

Notes and references

[a] *Beijing National Laboratory of Molecular Sciences, Key Laboratory of Green Printing, Institute of Chemistry, Chinese Academy of Sciences, Beijing, PR China. E-mail: lifb@iccas.ac.cn; yuangq@iccas.ac.cn; Fax: +86 10 62559373*

1. W. Wang, S. Wang, X. Ma and J. Gong, *Chem. Soc. Rev.*, 2011, **40**, 3703-3727.
2. A. Decortes, A. M. Castilla and A. W. Kleij, *Angew. Chem., Int. Ed.*, 2010, **49**, 9822-9837.
3. Y. Wang, X. Wang and M. Antonietti, *Angew. Chem., Int. Ed.*, 2012, **51**, 68-89.
4. S. Cao, J. Low, J. Yu and M. Jaroniec, *Adv. Mater.*, 2015, **27**, 2150-2176.
5. A. Thomas, A. Fischer, F. Goettmann, M. Antonietti, J.-O. Müller, R. Schlögl and J. M. Carlsson, *J. Mater. Chem.*, 2008, **18**, 4893- 4908.
6. R. Kuriki, K. Sekizawa, O. Ishitani and K. Maeda, *Angew. Chem., Int. Ed.*, 2015, **54**, 2406-2409.
7. J. Lin, Z. Pan and X. Wang, *ACS Sustain. Chem. Eng.*, 2014, **2**, 353-358.
8. W. J. Ong, L. L. Tan, S. P. Chai and S. T. Yong, *Chem. Commun.*, 2015, **51**, 858-861.
9. Y. He, Y. Wang, L. Zhang, B. Teng and M. Fan, *Appl. Catal., B,* 2015, **168-169**, 1-8.
10. P. Niu, Y. Yang, J. C. Yu, G. Liu and H. M. Cheng, *Chem. Commun.*, 2014, **50**, 10837-10840.
11. F. Goettmann, A. Thomas and M. Antonietti, *Angew. Chem., Int. Ed.*, 2007, **46**, 2717-2720.
12. J. Zhu, P. Xiao, H. Li and S. A. Carabineiro, *ACS Appl. Mater. Interfaces*, 2014, **6**, 16449-16465.
13. M. B. Ansari, B.-H. Min, Y.-H. Mo and S.-E. Park, *Green Chem.*, 2011, **13**, 1416- 1421.
14. M. North, R. Pasquale and C. Young, *Green Chem.*, 2010, **12**, 1514- 1539.

15. C. Maeda, T. Taniguchi, K. Ogawa and T. Ema, *Angew. Chem., Int. Ed.*, 2015, **54**, 134-138.
16. Q. Su, J. Sun, J. Wang, Z. Yang, W. Cheng and S. Zhang, *Catal. Sci. Technol.*, 2014, **4**, 1556- 1562.
17. J. Xu, F. Wu, Q. Jiang and Y.-X. Li, *Catal. Sci. Technol.*, 2015, **5**, 447-454.
18. J. Xu, F. Wu, Q. Jiang, J.-K. Shang and Y.-X. Li, *J. Mol. Catal. A-Chem.*, 2015, **403**, 77-83.
19. Z. Huang, F. Li, B. Chen, T. Lu, Y. Yuan and G. Yuan, *Appl. Catal., B*, 2013, **136-137**, 269-277.
20. Y. J. Zhang, A. Thomas, M. Antonietti and X. C. Wang, *J. Am. Chem. Soc.*, 2009, **131**, 50-51.
21. J. Xu, L. Zhang, R. Shi and Y. Zhu, *J. Mater. Chem. A*, 2013, **1**, 14766- 14772.
22. Z. Huang, F. Li, B. Chen and G. Yuan, *Catal. Sci. Technol.*, 2014, **4**, 4258-4264.
23. Z. Zhou, J. Wang, J. Yu, Y. Shen, Y. Li, A. Liu, S. Liu and Y. Zhang, *J. Am. Chem. Soc.*, 2015, **137**, 2179-2182.
24. S. Yang, Y. Gong, J. Zhang, L. Zhan, L. Ma, Z. Fang, R. Vajtai, X. Wang and P. M. Ajayan, *Adv. Mater.*, 2013, **25**, 2452-2456.
25. J. Zhang, M. Zhang, L. Lin and X. Wang, *Angew. Chem., Int. Ed.*, 2015, **54**, 6297-6301.
26. T. Y. Ma, Y. Tang, S. Dai and S. Z. Qiao, *Small*, 2014, **10**, 2382-2389.
27. J. Mao, T. Peng, X. Zhang, K. Li, L. Ye and L. Zan, *Catal. Sci. Technol.*, 2013, **3**, 1253- 1260.
28. X. Zhang, X. Xie, H. Wang, J. Zhang, B. Pan and Y. Xie, *J. Am. Chem. Soc.*, 2013, **135**, 18-21.
29. M. Shalom, S. Inal, C. Fettkenhauer, D. Neher and M. Antonietti, *J. Am. Chem. Soc.*, 2013, **135**, 7118-7121.
30. G. Zhang and X. Wang, *J. Catal.*, 2013, **307**, 246-253.
31. Y. Zheng, L. Lin, X. Ye, F. Guo and X. Wang, *Angew. Chem., Int. Ed.*, 2014, **53**, 11926-11930.
32. Q. Cai, J. Shen, Y. Feng, Q. Shen and H. Yang, *J. Alloys Compd.*, 2015, **628**, 372-378.
33. C. G. Li, L. Xu, P. Wu, H. Wu and M. He, *Chem. Commun.*, 2014, **50**, 15764-15767.
34. Y. Zhao, C. Yao, G. Chen and Q. Yuan, *Green Chem.*, 2013, **15**, 446-452.
35. J. N. Appaturi and F. Adam, *Appl. Catal., B*, 2013, **136-137**, 150-159.
36. F. Adam and M. S. Batagarawa, *Appl. Catal., A*, 2013, **454**, 164-171.
37. Z. Huang, F. Li, B. Chen, F. Xue, Y. Yuan, G. Chen and G. Yuan, *Green Chem.*, 2011, **13**, 3414-3422.
38. Z. Huang, F. Li, B. Chen, F. Xue, G. Chen and G. Yuan, *Appl. Catal., A*, 2011, **403**, 104-111.
39. X. Du, G. Zou, Z. Wang and X. Wang, *Nanoscale*, 2015, **7**, 8701-8706.
40. T. Sano, S. Tsutsui, K. Koike, T. Hirakawa, Y. Teramoto, N. Negishi and K. Takeuchi, *J. Mater. Chem. A*, 2013, **1**, 6489.
41. J. Li, B. Shen, Z. Hong, B. Lin, B. Gao and Y. Chen, *Chem. Commun.*, 2012, **48**, 12017-12019.
42. Y. Huang, Y. Wang, Y. Bi, J. Jin, M. F. Ehsan, M. Fu and T. He, *RSC Adv.*, 2015, **5**, 33254-33261.
43. Y. Xu, M. Xie, S. Huang, H. Xu, H. Ji, J. Xia, Y. Li and H. Li, *RSC Adv.*, 2015, **5**, 26281-26290.
44. R. Luo, X. Zhou, Y. Fang and H. Ji, *Carbon*, 2015, **82**, 1-11.
45. D. H. Lan, F. M. Yang, S. L. Luo, C. T. Au and S. F. Yin, *Carbon*, 2014, **73**, 351-360.
46. J. Sun, W. Cheng, Z. Yang, J. Wang, T. Xu, J. Xin and S. Zhang, *Green Chem.*, 2014, **16**, 3071-3078.
47. W. Chen, L. X. Zhong, X. W. Peng, R. C. Sun and F. C. Lu, *ACS Sustain. Chem. Eng.*, 2015, **3**, 147-152.
48. W. Cheng, B. Xiao, J. Sun, K. Dong, P. Zhang, S. Zhang and F. T. T. Ng, *Tetrahedron Lett.*, 2015, **56**, 1416-1419.

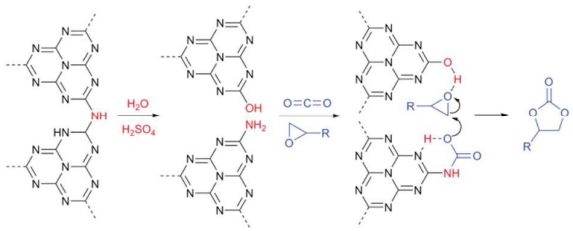

g-C_3N_4 activated by protonation using H_2SO_4 demonstrates a remarkable enhanced catalytic activity for cycloaddition of CO_2 and epoxide.